Asymmetries in strong-field photoionization by few-cycle laser pulses: Kinetic-energy spectra and semiclassical explanation of the asymmetries of fast and slow electrons

Szczepan Chelkowski and André D. Bandrauk
Laboratoire de Chimie Théorique, Faculté des Sciences, Université de Sherbrooke, Québec, Canada J1K 2R1
(Received 30 November 2004; published 26 May 2005)

Using numerical solutions of a time-dependent Schrödinger equation for a hydrogen atom in a linearly polarized few-cycle laser field, we calculate the left-right photoelectron kinetic-energy spectra measured by two opposing detectors placed along the laser polarization vector, with laser focus in the center. The fastest electrons show huge asymmetries strongly dependent on the laser carrier-envelope (CE) phase which confirms the recent theoretical results [D. B. Milosevic *et al.*, Opt. Express **11**, 1418 (2003)], obtained from a modified strong field approximation model which includes rescattering by the Coulomb potential. This asymmetry can also be explained by a simple semiclassical model in which the electron after tunneling through a potential barrier returns to the proton and is elastically backscattered in the presence of the laser field thus acquiring energy close $10U_p$ where U_p is the electron ponderomotive energy in the laser field. We also present a semiclassical interpretation of counterintuitive left-right asymmetries of slow electrons discussed in our previous work [Phys. Rev. A. **70**, 013815 (2004)]. Our analysis shows that the Coulomb attraction from the proton must be included in the standard tunneling model in order to account for the CE phase dependent angular asymmetry seen in our previous numerical calculations.

DOI: 10.1103/PhysRevA.71.053815 PACS number(s): 42.65.Re, 42.65.Ky, 32.80.Rm

I. INTRODUCTION

High-power ultrashort laser pulses with durations as short as few optical cycles are now available as research tools [1–4]. While long monochromatic pulses are completely characterized by their polarization, frequency, and the temporal shape of their envelope, short pulses require at least one additional parameter since the electric field envelope of a few cycle pulse varies significantly during one cycle. Typically the temporal shape of the laser electric field is represented as a product of Gaussian-like envelope times trigonometric function. The phase of this function becomes a physically important parameter for pulses shorter than four cycles and is called the carrier-envelope (CE) phase ϕ or the absolute phase. Recently, significant experimental progress has been achieved in stabilization of the CE phase [3,4], i.e., the relative phase between subsequent laser shots is controlled allowing us to perform experiments demonstrating various photoinduced phenomena, depending on the CE phase of an ultrashort laser pulse in gases [5,6] or on the metal surface [7]. When such a few cycle laser pulse interacts with atomic gas its CE phase will affect the following various laser induced processes [1]: harmonic generation [8], ionization (total ionization signal) [9], above threshold ionization (ATI), i.e., kinetic energy spectra [5,10,11], as well as photoelectron angular distributions [5,6,11–18]. The signature of the CE phase shows up in a particular simple way in the latter case, i.e., in asymmetries in angular distributions of photoelectrons. Both linearly and circularly polarized laser pulses lead to strong left/right asymmetries of photoelectrons which are very sensitive to the value of the CE phase. Recent theoretical investigations [18] show that asymmetries are strongest for most energetic electrons which have the kinetic energy close to $10U_p$. Here $U_p=I/4\omega^2$ is the electron's ponderomotive energy and I is the laser intensity (atomic units are used throughout). The first part of our paper is devoted to these asymmetries of fast electrons which show particularly simple patterns.

For long monochromatic laser pulses the CE phase of the laser pulse does not induce any measurable effect, in particular the angular photoelectron distributions $f(p_e,\theta)$ for each fixed value of the electron momentum $p_e=|\mathbf{p}_e|$ are symmetric, i.e., $f(p_e,\theta)=f(p_e,\pi-\theta)$ (where θ is the angle between the photoelectron momentum and the laser polarization vector) because of the symmetry of the monochromatic electric field and of the atom. Considerable variation of the field envelope during one cycle and the nonlinear response of the atom may lead to an asymmetry in photoelectron angular distributions, which can be used as a measurable signature of the absolute phase of the ultrashort laser pulse. Clearly we expect such an asymmetry to occur in an extreme case when the envelope variation is so fast that at the pulse maximum the electron can ionize classically over the potential barrier whereas in the next half cycle the barrier is too low for classical ionization. Similarly, an asymmetry is expected from the tunneling ionization mechanism, since due to the nonlinearity of the tunneling phenomenon only few central half-cycles of the pulse will contribute to the ionization signal. The basic physics of photoionization using strong, long wavelength pulses is well described using a tunneling model in which the recollision of the electron with the parent ion plays an essential role [19,20]. Usually these models are applicable when $U_p \gg I_p$, where I_p is the ionization potential, thus allowing us to neglect the Coulomb attraction during the electron's motion after its tunneling through the barrier and its eventual return to the core. Our recent studies based on the exact numerical solutions of the time-dependent Schrödinger equation (TDSE) for a hydrogen atom irradiated by a few cycle have shown that the standard tunneling model [19,20] [or the strong-field approximation (SFA) model [18]

in the first approximation] do not describe properly the asymmetries (obtained after integrating over all electron kinetic energy) since they do not include Coulomb attraction on the electron returning to the core. We present in the second part of this paper a classical simulation showing explicitly such an origin of the asymmetries measured by detectors which count all energies of electrons. Since the ATI spectrum has a two-plateau structure [21,22], the second plateau being 4–5 orders of magnitude weaker than the first one, the asymmetries investigated by us previously originate from slow electrons having kinetic energy smaller than $2U_p$. The first plateau of ATI spectrum comprises electrons of energy less than $2U_p$ whereas the second one extends up to $10U_p$. Our semiclassical calculations (Sec. IV) thus show that the addition of the Coulomb attraction to the standard tunneling model properly describes the above asymmetries predicted by simulations based on TDSE. In a sense these asymmetries appear to be counterintuitive since for the CE phase $\phi=0$ more electrons photoionize in the direction in which the field is strongest. A similar counterintuitive effect was found theoretically earlier in the two-color dissociative ionization of H_2^+ [15]. We have shown in [14] that asymmetry is "normal" (i.e., more electrons photoionize in the direction opposite to the strongest electric field) at higher intensities, i.e., in the barrier-suppression intensity range.

As in our previous work [14,16,17] we solve numerically the time-dependent Schrödinger equation (TDSE) for a hydrogen atom irradiated by a few cycle Ti:sapphire ($\lambda=800$ nm) laser pulse. Whereas previously we calculated only left-right asymmetries in angular distributions of all electrons (i.e., for an experiment in which electron energy is not measured and all are counted by both opposing detectors), we present here complete (left-right) ATI electron spectra. We analyze in detail their dependence on the CE phase, pulse duration, and its intensity. We confirm the validity of predictions obtained earlier from a simple semiclassical rescattering model and from a modified strong field approximation (SFA) model in which the electron rescattering is incorporated [18] to first order. In other words, we confirm the fact that the CE has a very simple and strong effect on fast electrons. Thus by controlling the CE phase we control the direction of photoemission of the fastest electrons in a very efficient and robust way: over ten times more electrons (having $8U_p-10U_p$ energy) can be sent to one side than another side of an atom along the laser polarization vector by simply changing the CE phase by π. Clearly, the asymmetry is much stronger when one measures only those fast electrons as compared to slower electron. However, this requires one to measure much weaker signals with high repetition rate and high stability of the CE phase which seems to be achievable, and such asymmetries have been used for measuring the laser CE phase [5]. Our study based on TDSE confirms the validity of this measurement. So far these asymmetries were evaluated either classically or using the SFA model which is valid only when U_p is larger than I_p. This requirement was not satisfied at intensity used in [18] $I=6\times10^{13}$ W/cm^2. Also note that the SFA model neglects all (except the ground state) an atom's bound states and in the rescattering term the Yukawa potential (instead of the Coulomb potential) was used. Therefore exact calculations based on the TDSE are necessary to confirm the predictions based on the SFA model at relatively low intensities.

II. BASIC EQUATIONS AND COMPUTATIONAL METHOD

We solve numerically the three-dimensional (3D) TDSE, using spherical coordinates r, θ, and atomic units (i.e., $e=\hbar=m_e=1$),

$$i\frac{\partial}{\partial t}\Psi(r,\theta,t) = -\frac{1}{2}\left(\frac{\partial^2}{\partial r^2}+\frac{2}{r}\frac{\partial}{\partial r}-\frac{L^2}{r^2}\right)\Psi + [-1/r + r\cos(\theta)E(t)]\Psi, \quad (1)$$

where L^2 is the square of angular momentum operator. Equation (1) describes the interaction of a hydrogen atom with a linearly polarized laser field $E(t)$ along the z axis. The numerical method we used is based on expansion in spherical harmonics (we use 51 harmonics) and it was described earlier by several authors [23]. Our integration grid was sufficiently large to avoid absorption at the boundary, we used $0<r<r_{\max}$, with $r_{\max}=6144$ Bohr. This grid size was sufficient since the total duration of our calculation was short. We used the spatial steps $dr=0.125$ Bohr and the integration step in time was 0.03 a.u.$=7\times10^{-19}$ s. We used the electric field $E(t)$ defined via the vector potential

$$A(t) = -c\varepsilon(t)\sin[\omega(t-t_M)+\phi]/\omega, \quad (2)$$

$$E(t) = -\frac{1}{c}\frac{\partial}{\partial t}A(t) = \varepsilon(t)\cos[\omega(t-t_M)+\phi] + E_{\rm cor}, \quad (3)$$

where t_M is the peak position, and

$$E_{\rm cor} = \sin[\omega(t-t_M)+\phi]\frac{\partial}{\partial t}\varepsilon_l(t)/\omega,$$

comes from the derivative of the envelope of the vector potential A. $E_{\rm cor}$ is small near the pulse maximum and is negligible for long pulses. For a single, one Ti-sapphire laser pulse, having the central wavelength at $\lambda_l=800$ nm, we used the envelope $\varepsilon_l(t)$ in the Gaussian form

$$\varepsilon(t) = I^{1/2}f_l(t), \quad f_l(t) = \exp[-2\ln(2)(t-t_M)^2/\tau_p^2], \quad 0<t<2t_M, \quad (4)$$

where I is the laser intensity in atomic units. We have chosen the total duration of the laser pulse to be 5 times longer than its full half-width of the intensity profile (FWHM) τ_p, i.e., $2t_M=5\tau_p$ is the total pulse duration. $\tau_p=3.9$ fs for pulses shown in Fig. 1. For few cycle pulses we do not use $E(t)$ represented as an arbitrary electric field envelope times trigonometric function since this may lead to a nonvanishing potential $A(t)$ at the end of the pulse which is equal to the area under the $E(t)$ function; a nonvanishing area would mean that the field has the dc component which could induce nonphysical asymmetries since the change of A leads to nonzero momentum acquired by the electron during the laser pulse. By contrast, our definition, Eq. (3), of $E(t)$ via $A(t)$ (which has an arbitrary envelope) guarantees that $A(0)=A(t_f)=E(0)=E(t_f)=0$. Figure 1 illustrates our definition of the

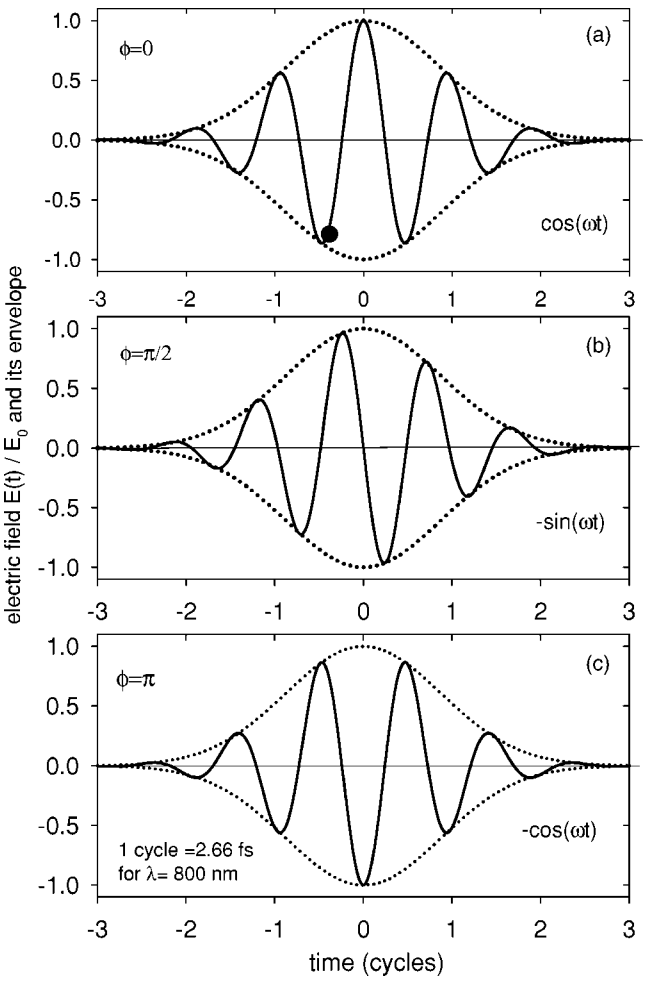

FIG. 1. Electric field $E(t)/E_0$ and its envelope $\varepsilon_0(t)/E_0$ as function of time in cycles for CE phases: (a) $\phi=0$; (b) $\phi=\pi/2$; (c) $\phi=\pi$. The central wavelength is $\lambda=800$ nm and the intensity profile half-width is $\tau_p=3.9$ fs. The bullet in (a) designates the tunneling time leading to the trajectory which ends with the electron energy $10U_p$.

absolute phase ϕ, Eq. (3): for $\phi_l=0$ the maxima of the field and envelope coincide [Fig. 1(a)], for $\phi_l=\pi/2$ the maximum of the envelope coincides with the zero of the field [Fig. 1(b)], and finally, for $\phi=\pi$ the maximum of the envelope occurs when the field reaches a minimum, Fig. 1(c): The numerical simulation was performed until the final time $t=t_f=2t_M+4$ cycles. The ATI electron spectra were calculated from the wave function $\Psi(r,\theta,t_f)$ by projecting its asymptotic part Ψ_{out} (in which only large r's are retained, see the definition below) on the plane wave $\varphi_f(\mathbf{r},\mathbf{p}_e)=(2\pi)^{-3/2}\exp(i\mathbf{p}_e\cdot\mathbf{r})$; first, we calculated the probability amplitude $a_f(\mathbf{p}_e)$ using

$$a_f(\mathbf{p}_e)=\langle\varphi_f|\Psi_{\text{out}}\rangle = (2\pi)^{-3/2}\int \exp(-i\mathbf{p}_e\cdot\mathbf{r})\Psi_{\text{out}}(r,\theta)r^2dr d\Omega, \quad (5)$$

where

$$\Psi_{\text{out}}=\begin{cases}0 & \text{for } r<r_0-b\\ \Psi(r,\theta,t_f)\cos^2[\pi(r_0-r)/(2b)] & \text{for } r_0-b<r<r_0\\ \Psi(r,\theta,t_f) & \text{for } r>r_0.\end{cases}$$

We used $r_0=128$ and $b=64$ Bohr. Such a choice smoothly removes most of the bound states from $\Psi(r,\theta,t_f)$, i.e., Ψ_{out} is mainly a superposition of continuum states. In Eq. (5) we use a plane wave instead of an exact Coulomb wave which is justified since the electron wave packet at $t=t_f$ (in particular its high energy part) has already reached a large distance, $r>500$ Bohr. Moreover, by using Ψ_{out}, defined by Eq. (6), in an integral present in Eq. (5), the plane wave is in fact used only at large distances, $r>r_0$. Thus $|a(\mathbf{p}_e)|^2p_e^2=|a(p_e,\theta_p)|^2p_e^2$ yield angle resolved momentum spectra (or energy spectra after dividing them by $p_e=dE_e/dp_e$). Instead of calculating the spectra at $\theta_p=0$ or π, as in [18], we integrated $|a(p_e,\theta_p)|^2|$ over θ_p within the detector angle assumed $0<\theta_p<\theta_0=0.0833\pi$ (which is equal to 15°). Thus we get the right S_{right} and left S_{left} ATI electron spectra measured by two opposing detectors which capture electrons with fixed energy $E_e=p_e^2/2$:

$$S_{\text{right}}(E_e)=2\pi\int_0^{\theta_0}d\theta_p\sin(\theta_p)p_e|a_f(p_e,\theta_p)|^2,$$

$$S_{\text{left}}(E_e)=2\pi\int_{\pi-\theta_0}^{\pi}d\theta_p\sin(\theta_p)p_e|a_f(p_e,\theta_p)|^2. \quad (6)$$

III. RESULTS: ATI SPECTRA

In Fig. 2 we plot ATI spectra defined by Eq. (6), for all energies, for the CE phase $\phi=0$ for laser intensities $I=6\times10^{14}$, 10^{14}, and 2×10^{14} W/cm^2, for which U_p is 3.6, 6.0, and 12 eV, respectively. Figure 3 shows the same plots but for the CE phase $\phi=\pi/2$. These figures show that the character of asymmetry depends strongly on the kinetic energy, in fact, e.g., in Fig. 2(a) we see three regimes. Low energy electrons ($E_e<15$ eV), which we show in more detail in Fig. 4, exhibit asymmetries discussed in [17]. We see in Fig. 2 that electrons having energy larger than $3U_p$ (11 eV at $I=6\times10^{13}$ W/cm^2) contribute little to the total signal (i.e., after integration over all electron energies). Thus asymmetries seen in Fig. 4 confirm our previous findings that for the CE phase $\phi=0$ more electrons go right, i.e., in the direction of the strongest field, see Fig. 1(a). This counterintuitive behavior (one might expect that since the electron charge is negative it should preferentially ionize to the opposite direction) of slow electrons is explained quantitatively in the next section where we present a modified tunneling model which includes the Coulomb attraction on the electron after tunneling. From the standard tunneling model one expects no-asymmetry in this case since the electric field is symmetric as function of $t-t_M$ where T_M is the pulse center time [15]. Such counterintuitive asymmetries, originating also from the Coulomb attraction, were observed originally in two-color dissociative ionization of H_2^+, which we modeled earlier using TDSE, non-Born-Oppenheimer numerical simulations [15].

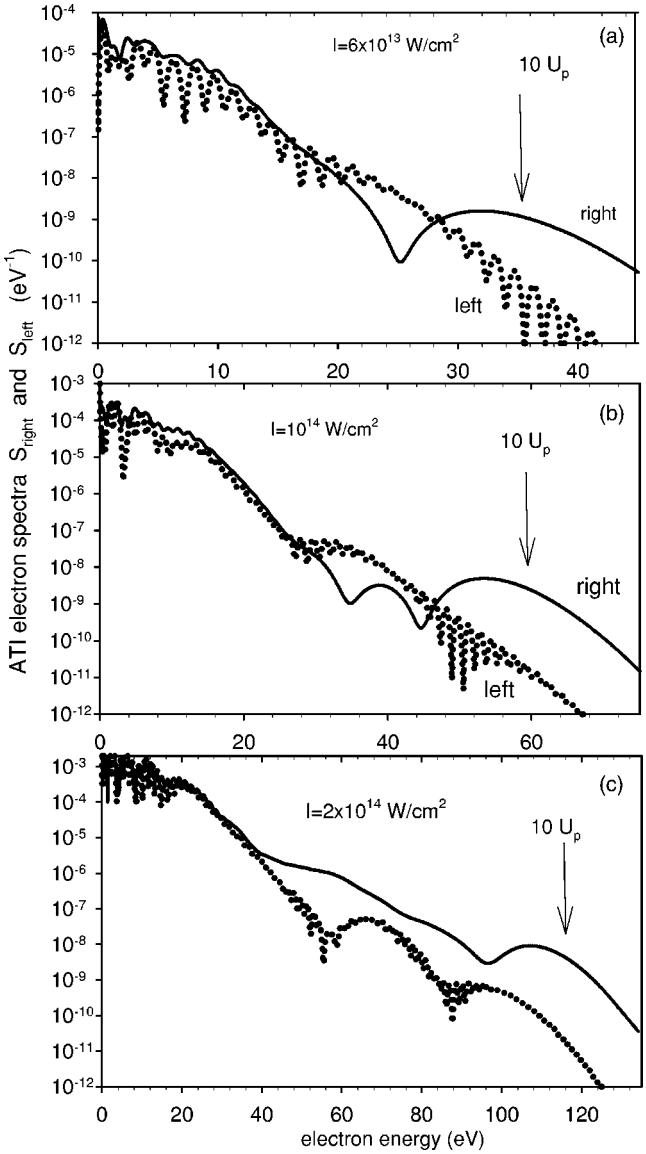

FIG. 2. Left and right ATI electron spectra $S_{\text{left}}(E_e)$ (dotted line) and $S_{\text{right}}(E_e)$ (solid line) defined by Eq. (6) for laser pulses having duration (FWHM) $\tau_p=3.9$ fs for the laser CE phase $\phi=0$ and for laser intensities (a) 6×10^{13}; (b) 10^{14}; and (c) 2×10^{14} W/cm^2.

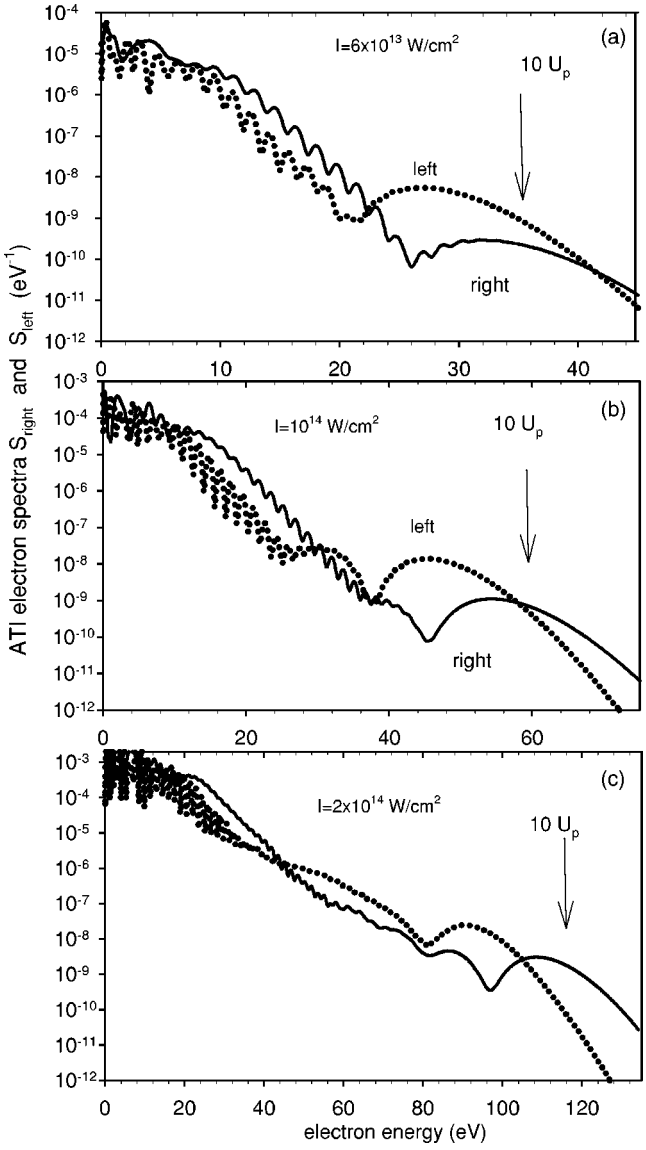

FIG. 3. Same as in Fig. 2 but for the laser CE phase $\phi=\pi/2$.

In Figs. 2(a) and 2(b) we see that the character of asymmetry changes at $E_e>5U_p$, to change again at $E_e>8U_p$. We note that around $10U_p$ the asymmetry is very strong and independent of laser intensity: nearly two orders of magnitude more fast electrons ionize to the right than to the left and this happens in the intensity range from 6×10^{13} to 2×10^{14} W/cm^2. These results are for the shortest pulses available so far, $\tau_p\simeq4$ fs. Figure 5 shows asymmetries for slightly longer pulses ranging from 5 to 6 fs. We note that for $\tau_p=5$ fs still ten times more fast electrons ($E_e\simeq10U_p$) ionize preferentially to the right than to the left, but we expect from the tendency seen in Fig. 5, as well as from the behavior of total asymmetries [14], that this asymmetry tends to disappear for laser pulses longer than τ_p longer than 7 fs. We also analyzed in more detail the dependence of the asymmetry on the absolute phase, see Figs. 6 and 7 which show ATI spectra of fast electrons at $I=6\times10^{13}$ W/cm^2 for phases from 0° to 157° (in intervals of 22.5°). Note that because of the symmetry of the field and of the Schrödinger equation [i.e., $E(t,\phi+180°)=-E(t,\phi)$, and the Hamiltonian H has the property $H(-z,\phi+180°)=H(z,\phi)$] the spectra exhibit the following symmetries: $S_{\text{right}}(E_e,\phi\pm180°)=S_{\text{left}}(E_e,\phi)$. Thus the spectrum for $\phi=180°$ (not shown) can be deduced from the spectrum shown in Fig. 6(a). The laser parameters are chosen the same as in [18] in which a modified SFA model was used. Despite the fact that the laser intensity is relatively low (below the applicability of SFA) the agreement between modified SFA calculations, see Fig. 2 in [18], and our results, shown in Figs. 6 and 7, is for fast electrons, $E_e>8U_p$, whereas the slower electron spectra differ considerably, probably because of the fact that SFA does not include excited bound states and in the rescattering term it uses a Yukawa potential. In general SFA is supposed to work when the electron energy is much larger than I_p which is 13.61 eV in our case. The difference between the present calculations

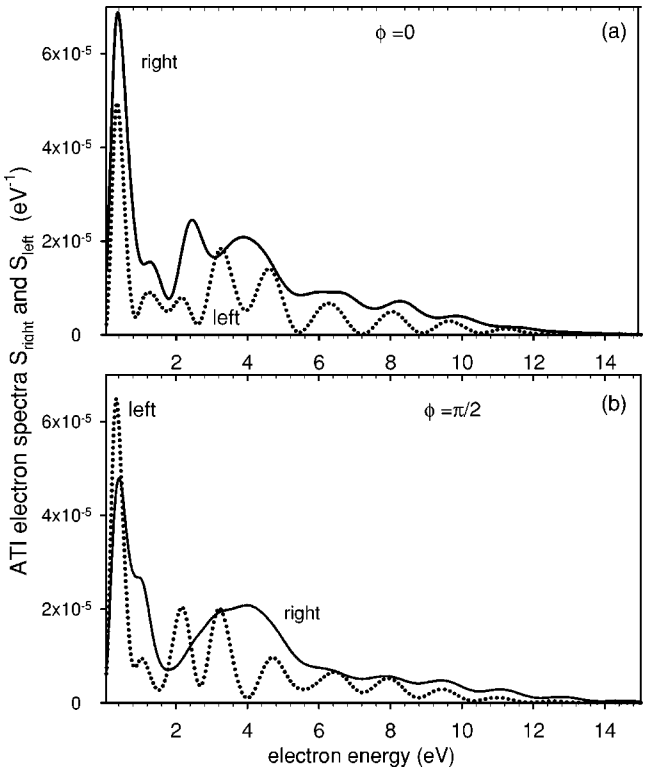

FIG. 4. Low energy part of the ATI spectra shown in Figs. 2(a) and 3(a).

and SFA low energy electron spectra may also originate from the fact that we integrated our angular distributions over the spherical angle θ_p from 0° to 15° whereas in [18] the spectra are obtained for a fixed angle $\theta_p=0$. We conclude from Figs. 6 and 7 that the asymmetry of $\simeq 10U_p$ electrons is largest for phase $\phi \simeq 160°$ (to the left) and (because of the symmetry with respect to the 180° shift) for $\phi \simeq -20°$ (to the right). Clearly, a significant control over direction of photoemission is achieved by varying the phase ϕ by 180°, which leads to a complete inversion of the photoemission direction of the fastest electrons. The origin of the asymmetry of these most energetic electrons is very simple and was explained earlier [18,22]: for ultrashort pulses such as in Fig. 1(a) there exists only one most likely classical trajectory leading to the $10U_p$ electron final energy. Such a trajectory originates from tunneling at the $t=\simeq -0.45$ cycle, i.e., close to a half-cycle preceding the central maximum, see Fig. 1(a), where this particular tunneling time is denoted by a bullet. Figure 3 in [18] shows that for $\phi=0$ this is the only tunneling time which leads to a trajectory ending with the maximal energy $\simeq 10U_p$. The electron after tunneling to the right at $t\simeq -0.45$ cycle returns to the nucleus at $t=\simeq 0.2$ cycle having the energy $\simeq 3U_p$. Then it can be elastically backscattered, i.e., it will move again to the right and gain more energy since during the half-cycle starting at the $t=0.25$ cycle the electron will be accelerated again by the negative electron field. Thus the electron can reach at the end of the pulse the energy $E_e \simeq 10U_p$. Since the pulse envelope varies rapidly only electrons ionizing to the right can reach such high energy, see Fig. 3 in [18]. Our calculations presented here (based on TDSE), as well as previous SFA calculations [18] confirm

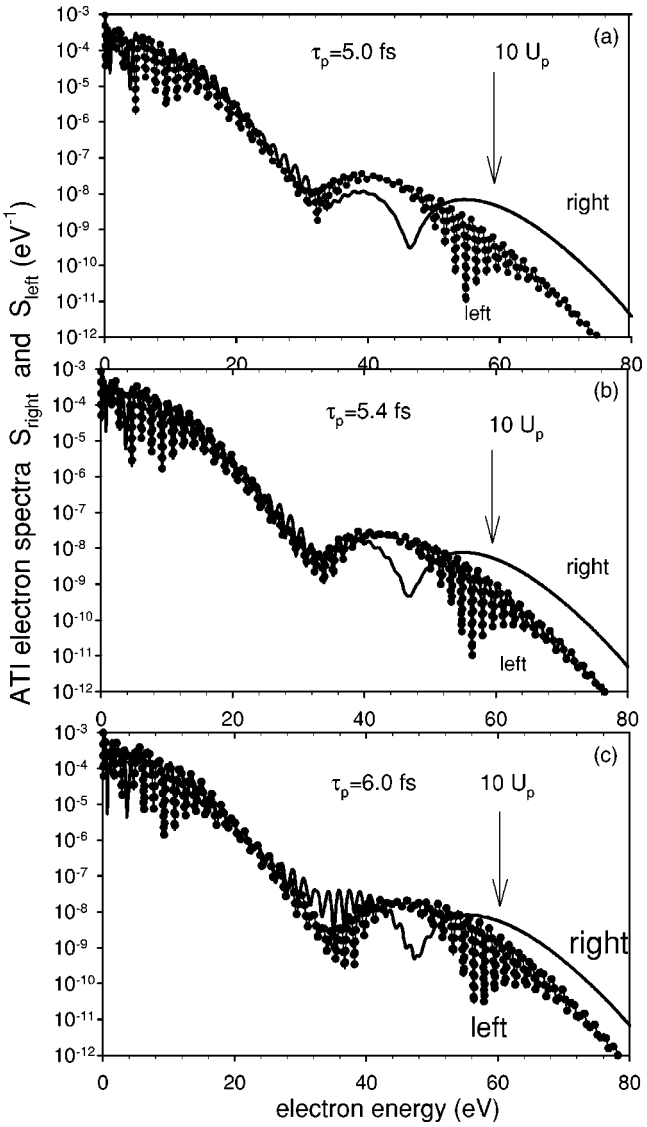

FIG. 5. Left and right ATI electron spectra $S_{\text{left}}(E_e)$ (dotted line) and $S_{\text{right}}(E_e)$ (solid line) defined by Eq. (6) for $I=10^{14}$, $\phi=0$ and for various pulse durations ranging from $\tau_p=5$ to $\tau_p=6.0$ fs.

this simple semiclassical scenario. This simple mechanism was already used for the measurement of the CE phase in the experiment [5].

IV. ASYMMETRIES OF SLOW ELECTRONS DESCRIBED BY A MODIFIED TUNNELING TWO-STEP MODEL

We provide, in the following, a simple semiclassical explanation of asymmetries of slow electrons (or asymmetries in total, integrated over the energy signal, predicted in our previous investigations based on the TDSE [17]) using a modified quasistatic atomic tunneling model. In this model ionization occurs in two steps. In the first step the electron ionizes with a tunneling rate R_{tun} which depends on the instantaneous field $E(t)$ [20],

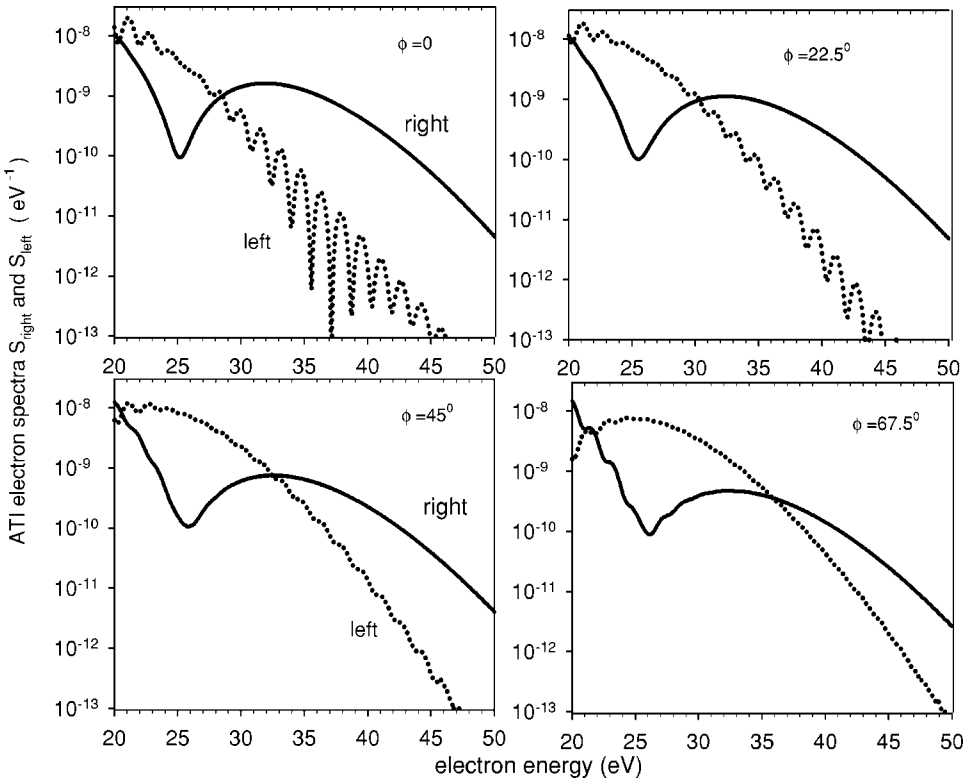

FIG. 6. Left and right ATI electron spectra (only its high energy part) $S_{\mathrm{left}}(E_e)$ (dotted line) and $S_{\mathrm{right}}(E_e)$ (solid line) defined by Eq. (6) for $I=6\times10^{13}$ W/cm^2, $\tau_p=3.6$ fs and for laser CE phases ϕ ranging from 0° to 67.5°.

$$R_{\mathrm{tun}}(E(t_0)) = \frac{4}{E(t_0)} \exp\left(-\frac{2}{3}\frac{1}{E(t_0)}\right). \tag{7}$$

In the second step, the electron moves as a classical particle according to the Newton equation of motion

$$\frac{d\mathbf{v}(t)}{dt} = -\mathbf{E}(t) - \boldsymbol{\nabla} V_C(|\mathbf{r}|), \tag{8}$$

where $V_C=-1/|\mathbf{r}|$ is the Coulomb potential. In a standard tunneling two-step model [20] the Coulomb potential V_C is

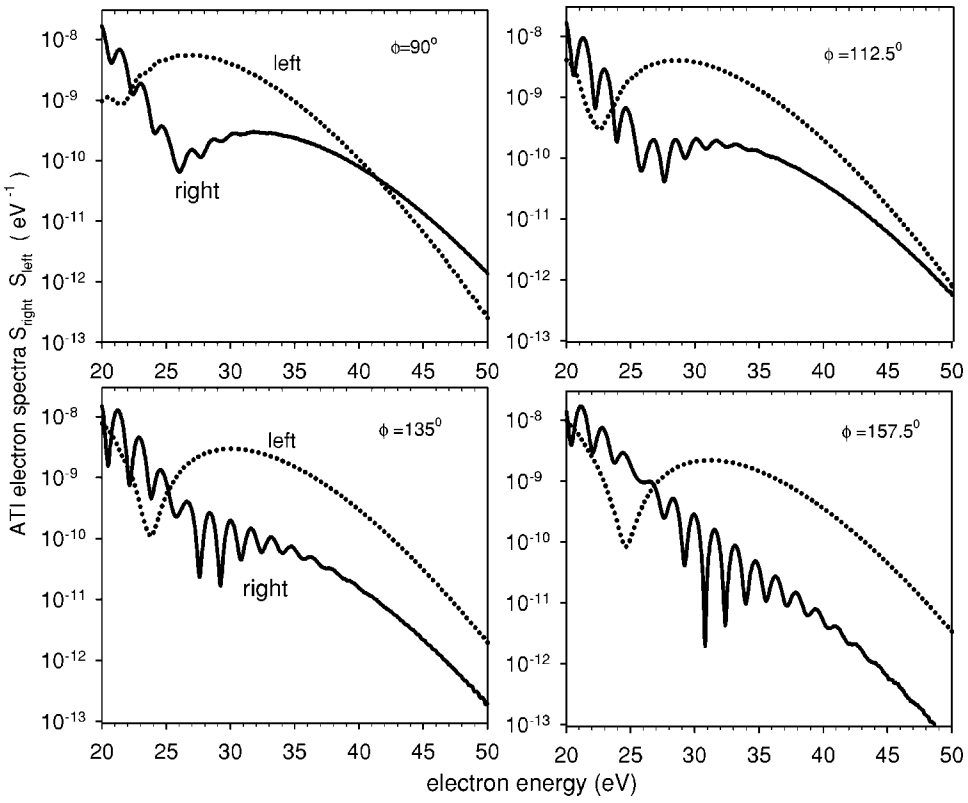

FIG. 7. For laser CE phases ϕ ranging from 90° to 157.5°. Note that because of symmetry the case of $\phi=180°$ can be deduced from the $\phi=0$ case shown in Fig. 6(a) by interchanging S_{right} and S_{left}.

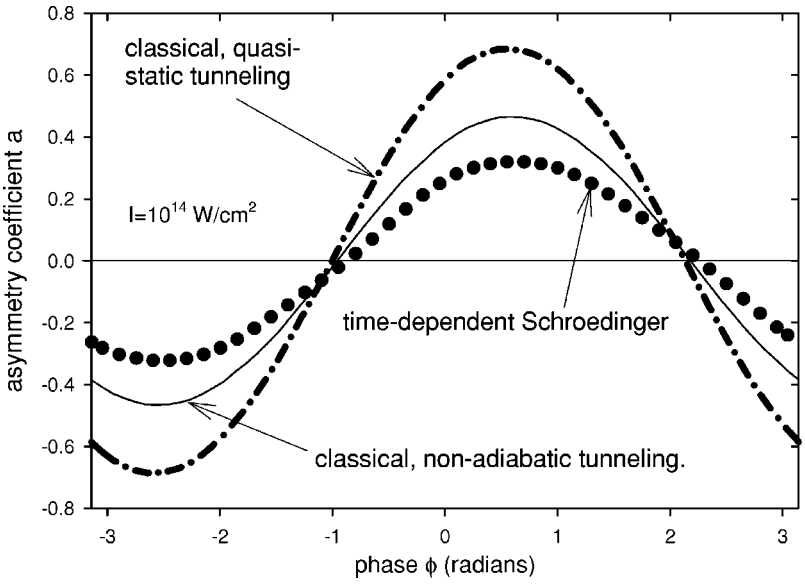

FIG. 8. Asymmetry coefficient defined by Eq. (12) as function of the CE phase ϕ for the laser intensity $I=10^{14}$ W/cm^2, $\tau_p=3.9$ fs (dash-dotted line) classical calculation using the quasistatic tunneling rate Eq. (7) (Solid line): classical calculation using the nonadiabatic rate; dotted line: quantum calculation based on the TDSE.

neglected, which allows us to obtain the following analytic solution of Eq. (8) for any shape of the electric field $E(t)=(-1/c)\partial A(t)/\partial t$:

$$\mathbf{v}(t)=\mathbf{v}(t_0)-\frac{1}{c}\mathbf{A}(t_0), \tag{9}$$

which is valid for any time after the turnoff of the field **A**. Usually one assumes that the initial velocity $\mathbf{v}(t_0)=$is zero. Thus, the electron final velocity is directly determined by the vector potential **A** at the tunneling time t_0. For the CE phase $\phi=0$ we thus simply get the final electron velocity [along the laser polarization, $\mathbf{E}\parallel Oz$)] $v_z=[\varepsilon(t_0)/\omega]\sin[\omega(t-t_M)]$ which is an asymmetric function of the variable $t-t_M$, where t_M is the time at the envelope maximum. Since the corresponding electric field $E(t)$, as well as the tunneling rate are symmetric functions of $t-t_M$, we conclude that this two-step model leads to symmetric photoemission for the CE phase $\phi=0$ (i.e., the same number of electrons photoionize to the left and to the right), contrary to what we found by solving TDSE, see Fig. 4(a) or our previous work [17], showing very large asymmetries occurring in the intensity range $3\times10^{13}-10^{14}$ W/cm^2 for $\phi=0$. We suggested in [17] that the disagreement between predictions from the two-step tunneling model and our results based on TDSE originates from the Coulomb attraction term neglected in the standard version of the model and is present in the Newton equations of motion. Therefore, in order to test the above hypothesis and in order to understand the physical mechanism of these asymmetries, as well as to explain the regularities of asymmetries as function of ϕ (in [16] we observe the simple sinelike dependence of normalized asymmetries on ϕ in the subtunneling regime) we solved numerically the Newton equation of motion (8) using a few thousands of various initial conditions [27]. More specifically, we solve Newton equations, using the Runge-Kutta method [24]), written in the following form:

$$\frac{d^2y}{dt^2}=-\frac{\partial V_C}{\partial y},\quad \frac{d^2z}{dt^2}=-\frac{\partial V_C}{\partial z}-E(t), \tag{10}$$

where for a hydrogen atom we used the softened Coulomb potential [25] $V_C(y,z)=1/\sqrt{1+y^2+z^2}$. Our present exact 3D classical dynamics of the electron motion was restricted to a two-dimensional (2D) motion by choosing initial positions, velocities, and the laser polarization vector to lie in the same plane defined by $x=0$ (there is no force component along the x axis for such initialized trajectories, therefore all such trajectories do not leave the yz plane). We initialized a few thousands trajectories in the following way: we selected 800 values of the tunneling time t_0 within the pulse center, $|t_0-t_M|<2.4$ cycle. For each t_0 the coordinate z_0 (of the electron after its jump through the barrier) was found from the equation: $V_C(z_0)+E(t_0)z_0-I_p=0$. Next, the Newton equations (10) were solved, by choosing for each t_0, z_0 180 initial transverse components of initial velocities $v_y(t_0)=v_T$, and we used the parallel component of the initial velocity $V_z(t_0)=0$. We assumed the following probability distribution of transverse velocities [25]:

$$P_T(v_T)=v_T\exp\left[-\left(\frac{v_T}{v_0}\right)^2\right],\quad 0<v_T<2v_0 \quad \text{where}$$
$$v_0=\left[\frac{I}{2I_p}\right]^{1/4}, \tag{11}$$

where the laser intensity and the ionization potential are in atomic units ($I_p=0.5$ for a hydrogen atom). The ionization signal P_{left}, P_{right} was computed by simply counting the trajectories which ionize within the angle $\theta_p=15°$, with respect to the z axis, to the right or left side, i.e., which ended at large z, $z>0$, or $z<0$, respectively. When counting trajectories, each one was weighed by the product of probabilities given by Eqs. (7) and (11). The calculations were repeated for a series of values of the laser CE phase ϕ. For each value of ϕ we calculated the asymmetry coefficient:

$$a=\frac{P_{\text{right}}-P_{\text{left}}}{P_{\text{right}}+P_{\text{left}}}. \tag{12}$$

Coefficients $a(\phi)$ are shown in Fig. 8 (dash–dotted line) and are compared with our previous quantum calculations (dotted line) [17]. Our classical calculation exaggerates considerably the asymmetry, but the general shape of the function $a(\phi)$, in

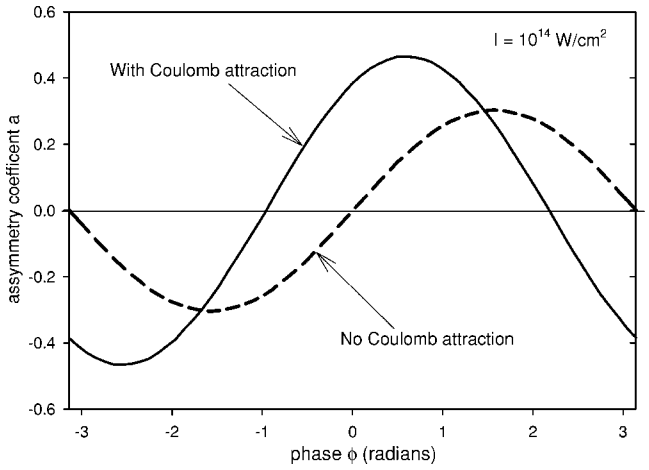

FIG. 9. Asymmetry coefficient obtained using the semiclassical model and the nonadiabatic rate for the laser intensity $I=10^{14}$ W/cm^2, $\tau_p=3.9$ fs. Solid line: with Coulomb attraction, using Eq. (8); dashed line: without the Coulomb attraction using Eq. (9).

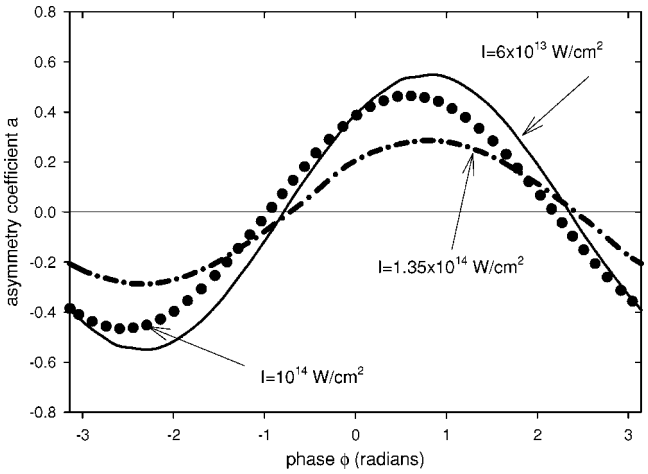

FIG. 10. Asymmetry coefficient obtained using the semiclassical model and the nonadiabatic rate for $\tau_p=3.9$ fs and for the laser intensities: $I=6\times10^{13}$, $I=10^{14}$, and for $I=1.35\times10^{14}$ W/cm^2.

particular coordinates corresponding to zero asymmetry and to the maximal asymmetry are correctly reproduced by our semiclassical model which includes Coulomb attraction at the classical stage of dynamics after the electron tunneling. Note that we used the standard tunneling rate formula which is valid for $\gamma=\sqrt{I_p/2U_p}\ll1$ whereas at $I=10^{14}$ W/cm^2 $\gamma=1.07$; therefore, we recalculated the coefficient of asymmetry using, instead of Eq. (7), the quasistatic rate which is valid for the Keldysh parameter $\gamma\simeq1$, and derived recently in [26]. More specifically, when counting ionized classical trajectories we used Eqs. (12), (17), and (18) from [26] instead of the standard tunneling formula (7) and the resulting symmetry coefficients $a(\phi)$ are shown in Fig. 8 (solid line). Clearly, we find that nonadiabatic corrections to the quasistatic model [26] improve the agreement with the exact quantum TDSE calculations. We also show in Fig. 9 the comparison of the same quasistatic asymmetries with calculations in which the electron trajectories are calculated as in standard two-step tunneling model (which neglects the Coulomb attraction), i.e., using analytically obtained trajectories, Eq. (9). Note, that in all classical calculations we assumed (for simplicity sake) that the initial parallel velocity $v_z(t_0)$ is zero. Figure 9 clearly shows the importance of Coulomb correction in semiclassical calculations. Finally we also show in Fig. 10 asymmetries for three intensities $I=6\times10^{13}$, 10^{14} and for 1.35×10^{14} W/cm^2.

The latter is the limiting intensity for purely tunneling ionization; at $I>1.5\times10^{14}$ W/cm^2 for t_0 close to the pulse maximum the electron can ionize over the barrier. Figure 10 demonstrates that, in general, asymmetries decrease with increasing intensities, as seen in our previous quantum simulations, and confirms our previous finding that the photoemission is symmetric for CE phases $\phi=-\pi/3+k\pi$, $k=0,\pm1,\pm2,\pm3$ [17]. Thus by including the Coulomb attraction in the electron classical dynamics after tunneling we reproduce using the modified two-step model the characteristic sinelike shapes of asymmetries predicted by our previous exact quantum calculations with considerable precision.

V. CONCLUDING REMARKS

We have presented a detailed investigation of spatial asymmetries in ATI spectra of photoelectrons induced by few cycles laser pulses. Our numerical calculations based on the exact TDSE for a H atom have confirmed previous results obtained within the framework of a modified SFA [18]. Simple asymmetry patterns for most energetic electrons ($E_e\simeq10U_p$) expected from the modified SFA theory also occur at relatively low intensities, $I\simeq6\times10^{13}$ W/cm^2, which are below the applicability range of the SFA model. At such intensities (which correspond to the nonperturbative regime lying between multiphoton and tunneling regime) the simulations based on the TDSE are most reliable. Our calculations presented here, based on TDSE and SFA calculations [18], confirm a very simple classical scenario leading to $10U_p$ photoelectrons in which the fastest electrons returning to the nucleus after tunneling are elastically backscattered and thus the electron is accelerated by two subsequent laser half-cycles, thus allowing us to achieve the energy $10U_p$. Most importantly, if the pulse duration is shorter than *two* cycles the electron is photoionized in the direction controlled by the laser CE phase: for the CE phase ϕ slightly below zero, 100 times faster electrons ionize to the right than to the left, whereas by changing the CE phase by 180° leads to the opposite asymmetry. Thus a very strong, robust control over the photoelectron direction is achieved. Clearly, the simplicity of the dependence of the asymmetry of most energetic electrons on the CE phase can be used as an important tool for measuring the CE phase, as suggested in [18] and used in the experiment [5]. Our studies also show that strong asymmetry of the fastest electrons ($E_e\simeq10U_p$) depends little on intensity in a wide intensity range: 6×10^{13} to 2×10^{14} W/cm^2, which is an important feature since averaging over focal intensities will not washout these asymmetries. We also note that these asymmetries are strong for pulse durations ranging from 4 to 6 fs.

In the second part of our paper we introduced a modified two-step semiclassical model in which we included the Cou-

lomb attraction on the electron after tunneling through the barrier. The resulting asymmetries, obtained by counting ionized trajectories, initialized at various few hundred tunneling times and with few hundred transverse initial velocities are close to the asymmetries calculated using TDSE. This result supports our previous hypothesis that asymmetries of slow electrons mainly originate from the Coulomb attraction on the electron escaping from the barrier after tunneling. In particular, for $\phi=0$ the electrons which tunnel slightly before the maximum of the electric field $E(t)$ do not ionize directly (as expected from the model which neglects the Coulomb attraction) but they either recombine with the ion or ionize in the opposite direction thus leading to the significant asymmetry whereas the standard SFA (or standard tunneling model) with no rescattering predict zero asymmetry at $\phi=0$. Summarizing, by including the Coulomb attraction in the electron dynamics after tunneling we reproduce the main features predicted by exact quantum calculations.

ACKNOWLEDGMENTS

The authors thank our summer student Marc Brosseau for assistance in solving numerically Newton equations. We also thank A. Apolonski and W. Becker (Berlin) for stimulating discussions.

[1] T. Brabec and F. Krausz, Rev. Mod. Phys. **72**, 545 (2000); A. Apolonski, A. Poppe, G. Tempea, Ch. Spielmann, Th. Udem, R. Holzwarth, T. W. Hansch, and F. Krausz, Phys. Rev. Lett. **85**, 740 (2000); Ch. Spielman, N. H. Burnett, S. Sartania, R. Koppitsch, M. Schnürer, C. Kan, M. Lenzner, P. Wobrauschek, and F. Krausz, Science **278**, 661 (1997).

[2] B. Schenkel, J. Biegert, U. Keller, C. Vozzi, M. Nisoli, G. Sansone, S. Stagira, S. De Silvestri, and O. Svelto, Opt. Lett. **28**, 1987 (2003).

[3] V. S. Yakovlev, P. Dombi, G. Tempea, C. Lemell, J. Burgdörfer, T. Udem, and A. Apolonski, Appl. Phys. B: Lasers Opt. **76**, 329 (2003).

[4] T. M. Fortier, D. J. Jones, and S. T. Cundiff, Opt. Lett. **28**, 2198 (2003).

[5] G. G. Paulus, F. Lindner, H. Walther, A. Baltuska, E. Goulielmakis, M. Lezius, and F. Krausz, Phys. Rev. Lett. **91**, 253004 (2003).

[6] G. G. Paulus *et al.*, Nature (London) **414**, 182 (2001).

[7] A. Apolonski, P. Dombi, G. G. Paulus, M. Kakehata, R. Holzwarth, Th. Udem, Ch. Lemell, K. Torizuka, J. Burgdörfer, T. W. Hänsch, and F. Krausz, Phys. Rev. Lett. **92**, 073902 (2004).

[8] A. de Bohan, Ph. Antoine, D. B. Milosevic, and B. Piraux, Phys. Rev. Lett. **81**, 1837 (1998).

[9] I. P. Christov, Appl. Phys. B: Lasers Opt. **70**, 459 (2000); Opt. Lett. **24**, 1425 (1999).

[10] D. B. Milosevic, G. G. Paulus, and W. Becker, Laser Phys. **13**, 948 (2003).

[11] P. Villoresi, G. G. Paulus, F. Grasbon, H. Walther, M. Nisoli, E. Priori, S. Stagira, G. Sansone, and S. De Silvestri, Laser Phys. **13**, 943 (2003).

[12] P. Dietrich, F. Krausz, and P. B. Corkum, Opt. Lett. **25**, 16 (2000).

[13] D. B. Milosevic, G. G. Paulus, and W. Becker, Phys. Rev. Lett. **89**, 153001 (2002).

[14] S. Chelkowski and A. D. Bandrauk, Phys. Rev. A **65**, 061802(R) (2002).

[15] A. D. Bandrauk and S. Chelkowski, Phys. Rev. Lett. **84**, 3562 (2000).

[16] S. Chelkowski, N. H. Shon, and A. D. Bandrauk, Laser Phys. **13**, 871 (2003).

[17] S. Chelkowski, A. D. Bandrauk, and A. Apolonski, Phys. Rev. A **70**, 013815 (2004).

[18] D. B. Milosevic, G. G. Paulus, and W. Becker, Opt. Express **11**, 1418 (2003).

[19] P. B. Corkum, N. H. Burnett, and F. Brunel, Phys. Rev. Lett. **62**, 1259 (1989).

[20] P. B. Corkum, Phys. Rev. Lett. **71**, 1994 (1993).

[21] G. G. Paulus, W. Nicklich, H. Xu, P. Lambropoulos, and H. Walther, Phys. Rev. Lett. **72**, 2851 (1994).

[22] G. G. Paulus, W. Becker, W. Nicklich, and H. Walther, J. Phys. B **27**, L703 (1994).

[23] P. L. Devries, J. Opt. Soc. Am. B **7**, 517 (1990); J. L. Krause, K. J. Schafer, and K. C. Kulander, Phys. Rev. A **45**, 4998 (1992).

[24] W. H. Press, S. A. Teukolsky, W. T. Vetterling, and B. P. Flannery, *Numerical Recipes in FORTRAN* (Cambridge University Press, New York, 1996).

[25] T. Brabec, M. Yu. Ivanov, and P. B. Corkum, Phys. Rev. A **54**, R2551 (1996); M. Yu. Ivanov, T. Brabec, and N. Burnett, *ibid.* **54**, 742 (1996).

[26] G. L. Yudin and M. Yu. Ivanov, Phys. Rev. A **64**, 013409 (2001).

[27] G. L. Yudin and M. Yu. Ivanov, Phys. Rev. A **63**, 033404 (2001).